

Model for Incomplete Reconnection in Sawtooth Crashes

M. T. Beidler and P. A. Cassak

Department of Physics, West Virginia University, Morgantown, WV, 26506, USA

A model for incomplete reconnection in sawtooth crashes is presented. The reconnection inflow during the crash phase of sawteeth self-consistently convects the high pressure core toward the reconnection site, raising the pressure gradient there. Reconnection shuts off if the diamagnetic drift speed at the reconnection site exceeds a threshold, which may explain incomplete reconnection. The relaxation of magnetic shear after reconnection stops may explain the destabilization of ideal interchange instabilities reported previously. Proof-of-principle two-fluid simulations confirm this basic picture. Predictions of the model compare favorably to data from the Mega Ampere Spherical Tokamak. Applications to transport modeling of sawteeth are discussed. The results should apply across tokamaks, including ITER.

Sawtooth crashes in tokamaks occur when the core temperature rapidly drops following a slow rise [1]. Large sawteeth are deleterious for fusion because they spoil confinement, while small sawteeth may be beneficial by limiting impurity accumulation [2]. Kadomtsev suggested the cause is the $m = 1, n = 1$ tearing mode [3], where m and n are poloidal and toroidal mode numbers. The predicted crash duration is the time it takes Sweet-Parker reconnection to process all available magnetic flux. This agreed with early experiments and simulations.

Soon after, cracks in the model appeared. Crash times in larger and hotter tokamaks were much faster than Kadomtsev's prediction [4, 5]. Also, Kadomtsev's model assumes all available magnetic flux reconnects (reconnection is "complete"), however experiments reveal that reconnection is usually incomplete [6]. Equivalently, the safety factor $q = rB_\varphi/R_0B_\theta$ does not exceed 1 everywhere after a crash, where R_0 and r are the major and minor radii and B_φ and B_θ are toroidal and poloidal magnetic fields.

Many models of incomplete reconnection exist, but there is no consensus on which, if any, is correct. Examples include stochastic magnetic fields [7], diamagnetic and pressure effects at the magnetic island [8–11], trapped high energy particles [12–14], a flattened q -profile [15], and the presence of shear flow [16, 17].

The uncertainty of the cause of incomplete reconnection impacts tokamak transport modeling. Low-dimensional transport models capture the sawtooth period and amplitude [18], but the fraction of flux reconnected is an input parameter rather than self-consistently calculated. A self-consistent theory of incomplete reconnection would improve tokamak transport models.

In this letter, we propose a model for incomplete reconnection in sawteeth due to the self-consistent dynamics of magnetic reconnection, building on established properties of diamagnetic effects [19]. After describing the model, we present numerical simulations confirming its key aspects. Then, we show that the model is consistent with data from the Mega Ampere Spherical Tokamak (MAST) [20]. Finally, applications and limitations of the result are discussed.

To understand why reconnection in Kadomtsev's model is complete, consider the $m = 1, n = 1$ reconnection plane sketched in Fig. 1. The reversed (auxiliary) magnetic field B_* is in red, the high pressure core is in grey, and the reconnection site is the black X. When re-

connection begins, outflow jets (in blue) are driven by tension in newly reconnected field lines. Mass continuity induces plasma inflow from upstream (also in blue). This flow convects more magnetic flux (if available) towards the reconnection site, which reconnects. Thus, reconnection is self-sustaining.

We argue that the key to explaining incomplete reconnection is the effect of reconnection dynamics on the pressure gradient at the reconnection site. Suppose the core is initially centered at the yellow X. The pressure gradient at the reconnection site (the green arrow) is radially inward and relatively weak. As the reconnection inflow self-consistently convects the core outward, the pressure gradient at the reconnection site increases. The outward motion of the core has long been seen in observations [5].

In the presence of a strong out-of-plane (guide) magnetic field B_h , in-plane pressure gradients lead to in-plane diamagnetic drifts, sketched in Fig. 1. Diamagnetic (ω_*) effects are known to stabilize linear and nonlinear tearing [21, 22], which continues to be actively studied [19, 23, 24]. It was shown [19] that reconnection does not occur if

$$|\mathbf{v}_{*i} - \mathbf{v}_{*e}|_{out} > v_{out}, \quad (1)$$

where v_{out} is the reconnection outflow speed, $\mathbf{v}_{*\alpha} = -\nabla p_\alpha \times \mathbf{B}/(q_\alpha n_\alpha B^2)$ is the diamagnetic drift velocity measured at the reconnection site for species $\alpha = i, e$, and the "out" subscript refers to the outflow direction.

We propose that the increase in v_{*i} and v_{*e} as the pressure gradient self-consistently increases due to reconnection causes the left-hand side of Eq. (1) to increase. If Eq. (1) is never satisfied, reconnection is complete. If the pressure gradient becomes large enough, reconnection ceases. Since Eq. (1) can be satisfied even when free magnetic energy remains, this provides a possible mechanism for incomplete reconnection. This model departs from previous ones [8–10] as it concerns pressure gradients at the reconnection site rather than the magnetic islands.

This model complements, and may explain key global features of, recent observations at MAST [20]. They observe that $|\nabla T_e|$ increases during a sawtooth period, peaking at the end of the crash (their Fig. 3), qualitatively consistent with the model. They also show that secondary ideal-MHD instabilities are destabilized at the end of the crash cycle. Reconnection would also play

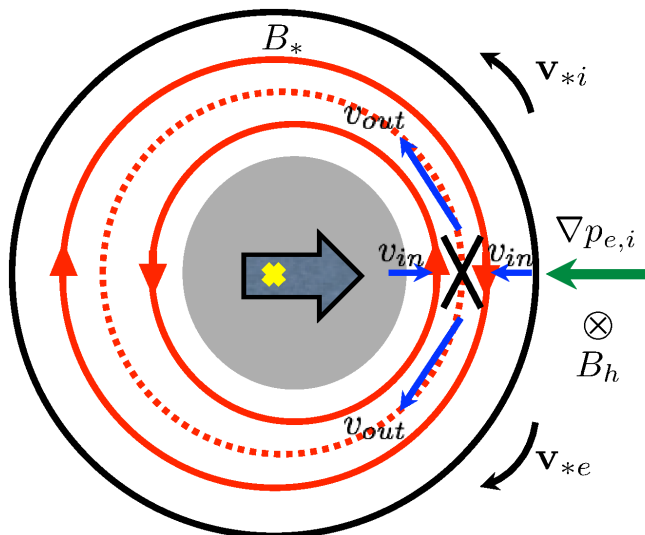


FIG. 1: (Color) Sketch of the $m = 1, n = 1$ reconnection plane. Reconnecting (auxiliary) magnetic fields B_* are in red with the rational surface r_s indicated by the dotted red line. Plasma inflows v_{in} and outflows v_{out} are in blue with the reconnection site at the black X. The grey core moves from its initial position centered at the yellow X. The pressure gradient is the green arrow. The helical guide field B_h and the diamagnetic drift velocities \mathbf{v}_{*i} and \mathbf{v}_{*e} are shown.

an important role in this process. When reconnection ceases, the electron-scale current sheet broadens, reducing the magnetic shear in a region where $|\nabla p|$ is large. Decreased shear is known to destabilize interchange instabilities (*e.g.* [25]).

To test the model, proof-of-principle numerical simulations are performed using F3D [26], a two-fluid code employing a two-dimensional slab geometry with periodic boundary conditions. This geometry is appropriate because motion in the plane normal to the guide magnetic field is well described in two dimensions, toroidal effects are not expected to play a role on the short time scales in question (tens of μs), and three-dimensional toroidal simulations employ unphysical forcing terms to obtain sawteeth [27]. These simulations do not contain toroidal effects which lead to secondary ideal-MHD instabilities [20] because this facet of the evolution is outside the scope of this study. Electron pressure is evolved assuming an adiabatic ideal gas with a ratio of electron specific heats $\gamma_e = 5/3$. Since the relative diamagnetic speed is the key parameter, ions are assumed cold for simplicity. Magnetic fields and mass densities are normalized to arbitrary values B_0 and ρ_0 , velocities to the Alfvén speed $c_{A0} = B_0/(4\pi\rho_0)^{1/2}$, lengths to the ion inertial length $d_{i0} = c/\omega_{pi} = (m_i^2 c^2/4\pi\rho_0 Z_{\text{eff}}^2 e^2)^{1/2}$, times to the ion cyclotron time $\Omega_{ci0}^{-1} = (Z_{\text{eff}} e B_0/m_i c)^{-1}$, electric fields to $E_0 = c_{A0} B_0/c$, and pressures to $p_0 = B_0^2/4\pi$, where m_i is the ion mass, c is the speed of light, e is the proton charge, and Z_{eff} is the effective atomic number.

The coordinate system has x parallel to the inflow (radial), y parallel to the outflow (poloidal), and z in the out-of-plane (toroidal) direction, invariant in the present two-dimensional simulations. The equilibrium has an in-

plane magnetic field profile of a double Harris sheet,

$$B_y(x) = \tanh\left(\frac{x - L_x/4}{w_0}\right) - \tanh\left(\frac{x + L_x/4}{w_0}\right) + 1,$$

where $L_x \times L_y = 102.4 \times 204.8$ is the system size and $w_0 = 0.5$ is the initial thickness of the current sheet. For this equilibrium, the toroidal mode number $n = 0$ manifestly, so the rational surfaces are $x_s = \pm L_x/4 = \pm 25.6$. We focus on a single mode because there is typically a dominant mode in sawteeth; the $n = 0$ mode is chosen for simplicity, but is not expected to alter the conclusions. The mass density is initially $\rho = 1$. The initial electron pressure profile is

$$p_e(x) = \frac{1}{2}(p_1 + p_2) + \frac{1}{2}(p_1 - p_2) \times \left[\tanh\left(\frac{x + 3L_x/8}{w_p}\right) - \tanh\left(\frac{x - 3L_x/8}{w_p}\right) - 1 \right].$$

The pressure gradient is localized near $x = \pm 3L_x/8 = \pm 38.4$ rather than at the rational surfaces x_s . Thus, p_e at the reconnection site is initially uniform. The length scale of the pressure gradient is $w_p = 2$. The guide magnetic field $B_z(x)$ has a mean value of 5 with a profile that ensures initial pressure balance, $p + B^2/2 = \text{constant}$.

The data we present are from simulations with a grid scale of $\Delta = 0.05$. A test simulation with $\Delta = 0.025$ confirms the resolution is sufficient. The equations employ fourth-order diffusion with coefficient $D_4 = 2 \times 10^{-5}$ to damp noise at the grid scale; D_4 has been varied to ensure the key physics is not sensitive to it. The electron to ion mass ratio is $1/25$. Simulations include no resistivity because experimental crash times are faster than collisional reconnection times. The presented simulations do not employ a parallel thermal conductivity, but test simulations with $\chi_{||} = 0.08$ reveal no significant changes. Tearing is initiated by a small coherent perturbation to the in-plane magnetic field of amplitude 0.01. It is known that secondary islands can spontaneously arise in reconnection simulations; due to symmetry, such islands would stay at the original X-line [28]. To prevent this, initial random magnetic perturbations of magnitude 2.0×10^{-5} break symmetry so secondary islands are ejected.

The principal simulation employs $p_1 = 5, p_2 = 25$ so v_{*e} will exceed v_{out} when the high pressure plasma convects in. Other simulation parameters are carefully chosen: $B_z \gg B_y$ as is relevant to sawteeth and p_e is large enough so the ion Larmor radius $\rho_s = c_s/\Omega_{ci}$ exceeds the electron skin depth $d_e = c/\omega_{pe}$, allowing fast reconnection to proceed [29, 30]. Here, $c_s = (\gamma_e Z_{\text{eff}} T_e/m_i)^{1/2}$ is the ion acoustic speed, and T_e is the electron temperature.

Upon evolving the system, Hall reconnection occurs initially and the high pressure plasma convects towards the reconnection site as expected. The reconnection rate E , measured as the time rate of change of magnetic flux between the X-line and O-line, is plotted as the solid (red) line in Fig. 2(a). It increases from zero to its expected value near 0.1 [31] by $t \sim 90$, where it reaches a steady-state with a single X-line. (The variation between $t = 40$ and 90 is due to transient secondary island formation

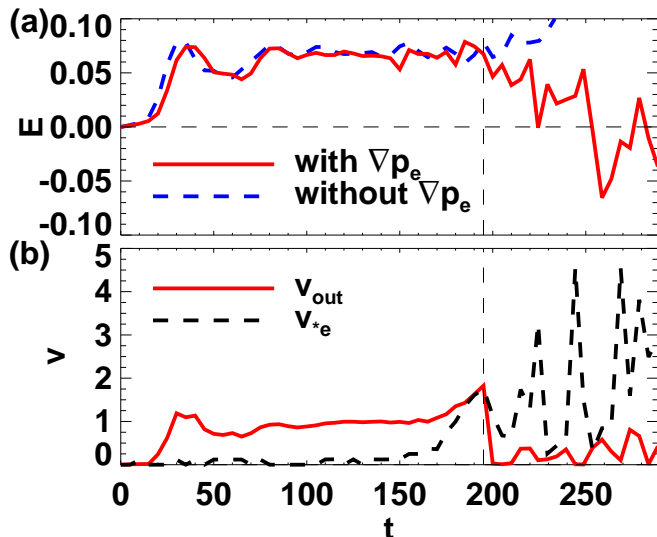


FIG. 2: (Color online) (a) Reconnection rate E as a function of time t with and without a pressure gradient. (b) Diamagnetic drift speed v_{*e} at the reconnection site and outflow speed v_{out} vs. t .

and coalescence.) At $t \simeq 195$, E begins decreasing. It decreases to below zero, where it fluctuates for a number of Alfvén crossing times. Thus, reconnection has shut off.

To determine the cause, the electron diamagnetic speed v_{*e} at the reconnection site is plotted as a function of time in Fig. 2(b) as the dashed (black) line. For comparison, the outflow speed v_{out} is plotted as the solid (red) line. Asymmetric outflows occur when there is a pressure gradient in the outflow direction [32], and since such gradients self-consistently generate here, v_{out} is calculated as the average of the maximum electron outflow speeds from either side of the reconnection site, averaged over $5d_e$ when turbulent.

Figure 2(b) reveals that v_{*e} is small initially, but increases in time once the pressure gradient reaches the reconnection site at $t \simeq 140$. It increases until it becomes comparable to v_{out} at $t \simeq 195$ (the vertical dashed line), the same time E begins to decrease. Therefore, reconnection is throttled when Eq. (1) is first satisfied.

To ensure diamagnetic effects occur, the out-of-plane current density J_z near the X-line is plotted in Fig. 3 (a) before ($t = 125$) and (b) after ($t = 180$) the pressure gradient arrives, with in-plane magnetic field lines superimposed. The guide field is in the $-z$ -direction and ∇p_e is in the $-x$ -direction. The reconnection site drifts in the $-y$ -direction, the direction of \mathbf{v}_{*e} . Note, a secondary instability (recently speculated to be a drift instability [33]) appears. The increased variability of v_{*e} and E after $t \simeq 205$ are attributed to this instability.

To ensure the observed effect is caused by the pressure gradient, simulations with other pressure profiles are performed. When there is no gradient with $p_1 = p_2 = 5$, there is no decrease in E , plotted as the dashed (blue) line in Fig. 2(a). The same is true for $p_1 = p_2 = 25$ (not plotted). When $p_1 = 5, p_2 = 7$, no drop in reconnection rate is observed because the maximum v_{*e} only reaches ~ 1 , but $v_{out} \sim 2$ so Eq. (1) is never satisfied. In sum-

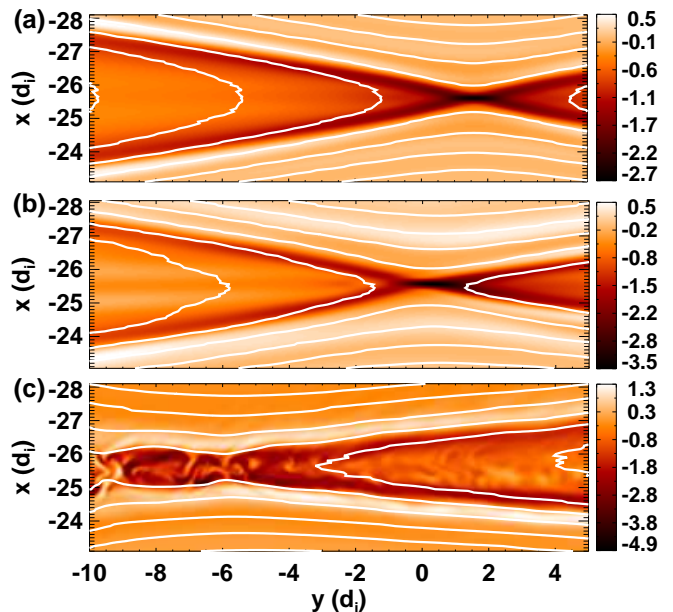


FIG. 3: (Color) Out-of-plane current density J_z zoomed in near the X-line with magnetic field lines superimposed (a) before ($t = 125$), (b) after ($t = 180$), and (c) significantly after ($t = 210$) the pressure gradient reaches the reconnection site. The x and y axes correspond to the radial and poloidal directions, respectively.

mary, the simulations confirm the basic prediction of the model: reconnection ceases when large enough pressure gradients self-consistently convect into the reconnection site despite the presence of free magnetic energy.

Post-cessation features are important for the subsequent dynamics. Figure 3(c) shows J_z significantly after the pressure gradient reaches the reconnection site ($t = 210$). The current layer clearly broadens as reconnection stops, reducing the magnetic shear at the reconnection site, as evidenced by the negative reconnection rate in Fig. 2(a). The reduced shear would make the system more prone to interchange instabilities, which were argued to occur in Ref. [20].

Equation (1) provides a quantitative prediction of the conditions at the end of sawteeth; we assess it with data from MAST [20]. To transform into the plane of reconnection perpendicular to the $m = 1, n = 1$ helical direction, the reconnecting (auxiliary) field B_* is related to the toroidal B_φ and poloidal B_θ fields by

$$B_*(r) = B_\theta - \left(\frac{r}{R_0}\right) B_\varphi. \quad (2)$$

At MAST, $R_0 = 0.85$ m [34] while $B_\varphi \simeq 0.4$ T and $B_\theta \simeq 0.15$ T [35]. The rational surface r_s is where $B_* = 0$ in Eq. (2), which gives $r_s \simeq 0.32$ m. This result agrees well with Fig. 1(a) of Ref. [20]. The helical guide field at r_s is $B_h = B_\varphi(1 + r_s/R_0) \simeq 0.55$ T.

To test the model, Eq. (1) must be evaluated at the end of the sawtooth crash. The outflow speed scales with c_{Ae} , the electron Alfvén speed based on the field B_{*e} upstream of the electron current layer. Assuming the large guide field limit with $B_h \gg B_*$ in the vicinity of

r_s , the thickness of the electron current layer scales as the electron Larmor radius $\rho_e = v_{th,e}/\Omega_{ce}$ [36], where $v_{th,e} = (\gamma_e T_e/m_e)^{1/2}$ is the electron thermal speed and $\Omega_{ce} = eB/m_e c$ is the electron cyclotron frequency. Using $T_e \simeq 500$ eV at r_s [20] and $\gamma_e = 5/3$, we find $\rho_e \simeq 0.013$ cm. To find B_{*e} , we evaluate Eq. (2) at $r_s \pm 2\rho_e$ [37], which gives $B_{*e} \simeq 5.9 \times 10^{-5}$ T, justifying the strong guide field assumption. Using this value gives $v_{out} \approx 14.2$ km/s, where $n_e \simeq 6 \times 10^{19}$ m $^{-3}$ is estimated from Fig. 2 in Ref. [20].

To estimate v_{*e} , note $|\nabla p_e|/n_e = |\nabla T_e| + T_e(|\nabla n_e|/n_e)$. The right-hand side is estimated at the end of the crash from Figs. 1(e), 2 and 3 of Ref. [20] to be $|\nabla p_e|/n_e \simeq 7400$ eV/m. Then, the electron diamagnetic speed is $v_{*e} = |\nabla p_e|/(qn_e B_h) \approx 13.5$ km/s. Equation (1) includes ion diamagnetic effects, but complementary ion data is unavailable [35]. Assuming the ion temperature has a similar profile as the electrons with $T_e > T_i$, we expect $v_{*e} < |v_{*i}| + |v_{*e}| < 2v_{*e}$. Thus, the two speeds agree rather well, showing the agreement with the data is also quantitative.

As a further consistency check, we compare the speed of the core to the inflow speed. The the core's speed is estimated from Figs. 1(d-f) of Ref. [20] by dividing its displacement ($\simeq 0.08$ m) by the elapsed time ($\simeq 0.04$ ms), giving a speed of ~ 2 km/s. The reconnection inflow speed scales like $0.1c_{Ai}$ [26], where c_{Ai} is the ion Alfvén speed based on the field B_{*i} upstream of the ion current layer. The ion layer thickness with a large guide field scales like the ion Larmor radius ρ_s [21]. Using $Z_{eff} \sim 1$ [38] and $m_i = 2m_p$ for a deuterium plasma [34], we find $\rho_s \sim 0.77$ cm. As in the calculation of B_{*e} , we evaluate Eq. (2) at $r_s \pm 2\rho_s$, giving $B_{*i} = 6.7 \times 10^{-3}$ T. Then, $c_{Ai} \approx 13$ km/s, so the inflow speed is $\simeq 1.3$ km/s. Thus, the inflow speed is comparable to the speed of the core, as predicted.

For tokamak applications, Eq. (1) may be recast in terms of more familiar quantities. Assuming $v_{out} \sim c_{Ae}$ in Eq. (1) and rewriting Eq. (2) in terms of q and ex-

panding to lowest order in r for a small displacement ($2\rho_e$) from r_s , $B_{*e} \simeq B_\theta q' 2\rho_e$, where the prime denotes a radial derivative. Thus, Eq. (1) becomes

$$\frac{1}{eB_h} \left| \frac{p'_i}{Z_{eff} n_i} + \frac{p'_e}{n_e} \right| > \frac{2\rho_e B_\theta}{\sqrt{4\pi m_e n_e}} q', \quad (3)$$

where all quantities are evaluated at r_s . This expression is reminiscent of the condition on p' and q' for suppression of sawteeth derived from linear tearing theory [21, 39].

In conclusion, we have described a model for incomplete reconnection in sawtooth crashes, tested the basic physics with numerical simulations, and shown it is consistent with data from MAST. Interestingly, recent simulations of sawteeth revealed complete reconnection in MHD, but incomplete reconnection in extended-MHD with electron and ion diamagnetic effects [27, 40]; the present result may be relevant. Equation (1) may be useful for low-dimensional transport modeling, which currently use ad hoc models to achieve incomplete reconnection [41]. The present results are machine independent, so they should apply both to existing tokamaks and future ones such as ITER.

In future studies, the model should be tested with other extended-MHD effects such as ion diamagnetic effects and higher $\chi_{||}$. The restriction on toroidal mode number n should be relaxed. The effect of the electron pressure profile on the dynamics and the secondary (drift) instability should be addressed; this may need to utilize particle-in-cell simulations. Including 3D toroidal geometry is critical for exploring secondary ideal-MHD instabilities. Comparisons to multiple tokamak discharges should be done to test the scaling.

We thank I. T. Chapman for providing MAST data and thank J. F. Drake, D. C. Pace, M. A. Shay, and M. Swisdak for helpful conversations. The authors gratefully acknowledge support by NSF grant PHY-0902479. This research used resources at National Energy Research Scientific Computing Center.

-
- [1] S. von Goeler, W. Stodiek, and N. R. Sautoff, Phys. Rev. Lett. **33**, 1201 (1974).
[2] T. C. Hender, J. C. Wesley, J. Bialek, A. Bondeson, A. H. Boozer, R. J. Buttery, A. Garofalo, T. P. Goodman, R. S. Granetz, Y. Gribov, et al., Nucl. Fusion **47**, S128 (2007).
[3] B. B. Kadomtsev, Sov. J. Plasma Phys. **1**, 389 (1975).
[4] A. W. Edwards, D. J. Campbell, W. W. Engelhardt, H. U. Farhbach, R. D. Gill, R. S. Granetz, S. Tsuji, B. J. D. Tubbing, A. Weller, J. Wesson, et al., Phys. Rev. Lett. **57**, 210 (1986).
[5] M. Yamada, F. M. Levinton, N. Pomphrey, R. Budny, J. Manickam, and Y. Nagayama, Phys. Plasmas **1**, 3269 (1994).
[6] H. Soltwisch, Plasma Phys. Control. Fusion **34**, 1669 (1992).
[7] A. J. Lichtenberg, K. Itoh, S. I. Itoh, and A. Fukuyama, Nucl. Fusion **32**, 495 (1992).
[8] D. Biskamp, Phys. Rev. Lett. **46**, 1522 (1981).
[9] D. Biskamp and T. Sato, Phys. Plasmas **4**, 1326 (1997).
[10] W. Park, D. A. Monticello, and T. K. Chu, Phys. Fluids **30**, 285 (1987).
[11] X. Wang and A. Bhattacharjee, Phys. Plasmas **2**, 171 (1995).
[12] B. Coppi, R. J. Hastie, S. Migliuolo, F. Pegoraro, and F. Porcelli, Phys. Lett. A **132**, 267 (1988).
[13] R. B. White, M. N. Bussac, and F. Romanelli, Phys. Rev. Lett. **62**, 539 (1989).
[14] F. Porcelli, Plasma Phys. Control. Fusion **33**, 1601 (1991).
[15] J. A. Holmes, B. A. Carreras, and L. A. Charlton, Phys. Fluids B **1**, 788 (1989).
[16] R. G. Kleva, Phys. Fluids B **4**, 218 (1992).
[17] R. G. Kleva and P. N. Guzdar, Phys. Plasmas **9**, 3013 (2002).
[18] F. Porcelli, D. Boucher, and M. N. Rosenbluth, Plasma Phys. Control. Fusion **38**, 2163 (1996).
[19] M. Swisdak, J. F. Drake, M. A. Shay, and B. N. Rogers, J. Geophys. Res. **108**, 1218 (2003).
[20] I. T. Chapman, R. Scannell, W. A. Cooper, J. P. Graves, R. J. Hastie, G. Naylor, and A. Zocco, Phys. Rev. Lett.

- 105**, 255002 (2010).
- [21] L. Zakharov, B. Rogers, and S. Migliuolo, *Phys. Fluids B* **5**, 2498 (1993).
- [22] B. Rogers and L. Zakharov, *Phys. of Plasmas* **2**, 3420 (1995).
- [23] K. Germaschewski, A. Bhattacharjee, C. S. Ng, X. Wang, and L. Chacon, in *Bull. Am. Phys. Soc.* (2006), vol. 51, p. 312.
- [24] A. Bhattacharjee, K. Germaschewski, L. Nei, and H. Yang, in *Eos Trans. AGU* (AGU, San Francisco, 2008), vol. 89(53) of *Fall Meet. Suppl.*, pp. Abstract SM21B-04.
- [25] J. P. Freidberg, *Ideal Magnetohydrodynamics* (Springer, 1987).
- [26] M. A. Shay, J. F. Drake, M. Swisdak, and B. N. Rogers, *Phys. Plasmas* **11**, 2199 (2004).
- [27] J. A. Breslau, C. R. Sovinec, and S. C. Jardin, *Commun. Comput. Phys.* **4**, 647 (2008).
- [28] N. F. Loureiro, S. C. Cowley, W. D. Dorland, M. G. Haines, and A. A. Schekochihin, *Phys. Rev. Lett.* **95**, 235003 (2005).
- [29] A. Y. Aydemir, *Phys. Fluids B* **4**, 3469 (1992).
- [30] B. N. Rogers, R. E. Denton, J. F. Drake, and M. A. Shay, *Phys. Rev. Lett.* **87**, 195004 (2001).
- [31] M. A. Shay, J. F. Drake, B. N. Rogers, and R. E. Denton, *Geophys. Res. Lett.* **26**, 2163 (1999).
- [32] N. A. Murphy, C. R. Sovinec, and P. A. Cassak, *J. Geophys. Res.* **115**, A09206 (2010).
- [33] J. F. Drake (2011), Private Communication.
- [34] L. C. Appel, T. Fülöp, M. J. Hole, H. M. Smith, S. D. Pinches, R. G. L. Vann, and the MAST team, *Plasma Phys. Control. Fusion* **50**, 115011 (2008).
- [35] I. T. Chapman (2011), Private Communication.
- [36] R. Horiuchi and T. Sato, *Phys. Plasmas* **4**, 277 (1997).
- [37] B. D. Jemella, M. A. Shay, J. F. Drake, and B. N. Rogers, *Phys. Rev. Lett.* **91**, 125002 (2003).
- [38] M. R. Tournianski, R. J. Akers, P. G. Carolan, and D. L. Keeling, *Plasma Phys. Control. Fusion* **47**, 671 (2005).
- [39] F. M. Levinton, L. Zakharov, S. H. Batha, J. Manickam, and M. C. Zarnstorff, *Phys. Rev. Lett.* **72**, 2895 (1994).
- [40] J. A. Breslau, S. C. Jardin, and W. Park, *Phys. Plasmas* **14**, 056105 (2007).
- [41] G. Bateman, C. N. Nguyen, A. H. Kritz, and F. Porcelli, *Phys. Plasmas* **13**, 072505 (2006).